Photostable Carbon Dots with Intense Green Emission in an Open Reactor Synthesis

G. Minervini[a,b,c], A. Panniello[c]*, A. Madonia[c], C.M. Carbonaro[d], F. Mocci[e], T. Sibillano[f], C. Giannini[f], R. Comparelli[c], C. Ingrosso[c], N. Depalo[c], E. Fanizza[b,c], M.L. Curri[b,c], M. Striccoli[c]*

[a] Department of Electrical and Information Engineering, Polytechnic of Bari, Via E. Orabona 4, Bari, 70126, Italy; gianluca.minervini@poliba.it
[b] Department of Chemistry, University of Bari "Aldo Moro", Via Orabona 4, Bari, 70126, Italy; elisabetta.fanizza@uniba.it; marialucia.curri@uniba.it;
[c] CNR-IPCF Bari Division, c/o Chemistry Department, University of Bari "Aldo Moro", Via Orabona 4, Bari, 70126, Italy; a.madonia@ba.ipcf.cnr.it; r.comparelli@ba.ipcf.cnr.it; c.ingrosso@ba.ipcf.cnr.it; n.depalo@ba.ipcf.cnr.it;
[d] Department of Physics, University of Cagliari, SP8, Monserrato, 09042, Italy; cm.carbonaro@dsf.unica.it;
[e] Department of Chemical and Geological Sciences, University of Cagliari, SP8; fmocci@unica.it;
[f] Institute of Crystallography (IC), CNR, Via Amendola 122, Bari, 70126, Italy; teresa.sibillano@ic.cnr.it; cinzia.giannini@ic.cnr.it

* corresponding authors: Tel +39 080 5442027; Email: a.panniello@ba.ipcf.cnr.it; m.striccoli@ba.ipcf.cnr.it

Abstract

Carbon dots (CDs) are novel fluorescent nanoparticles that combine intense emission of visible light with eco-friendly and inexpensive carbon-based composition. In this work, CDs are synthesized trough a glycothermal treatment of resorcinol (1,3-hydroxybenzene) in air atmosphere. The presence of catalysts (NaOH and H_2SO_4) increases the reaction rate, promoting a faster and massive production of nanoparticles. The spectroscopic monitoring of fluorescence during CD synthesis, supported by a DFT study, allows to depict the formation and structural evolution of OH terminated polycyclic aromatic hydrocarbons (PAHs) from resorcinol polycondensation. In purified CDs, PAHs embedded in the amorphous carbogenic core are responsible for an intense green fluorescence emission with a quantum yield up to ~ 40%. Such band exhibits high resistance to UV photobleaching, attributed to the physical protection of the carbogenic matrix. Finally, adding a strong acid/base to the CD solution, the CD fluorescence can be cyclically quenched/restored (due to reversible aggregation), suggesting the convenient use of such CDs in on/off sensors or stimulus-responding devices.

Keywords: Carbon dot, Open reactor, Catalyzed green synthesis, DFT, Fluorescence spectroscopy, Photobleaching.

Abbreviations: Carbon Dots (CDs), Polycyclic Aromatic Hydrocarbons (PAHs), Photoluminescence (PL), Ethylene Glycol (EG), Photoluminescence Quantum Yield (PLQY), CDs synthesized without added catalysts (n-CDs), CDs synthesized with base catalysts (b-CDs), CDs synthesized with acid catalysts (a-CDs), Transmission Electron Microscopy (TEM), Wide Angle X-ray Scattering (WAXS), Grazing Incidence Wide Angle X-ray Scattering (GIWAXS), Fourier-Transform Infrared (FT-IR), Time-Resolved Photoluminescence (TRPL), Time Correlated Single Photon Counting (TCSPC), Density Functional Theory (DFT), Self-Consistent Reaction Field (SCRF), Polarizable Continuum Model (PCM), Integral Equation Formalism Polarizable Continuum Model (IEFPCM), Highest Occupied Molecular Orbital (HOMO), Lowest Unoccupied Molecular Orbital (LUMO).

1. Introduction

Fluorescent carbon nanoparticles, usually named Carbon Dots (CDs), have recently emerged in the panorama of luminescent materials, which already includes organic fluorescent molecules, rare earth-based phosphors, semiconductor and perovskites quantum dots [1–3]. Indeed, CDs combine low cost effectiveness, biocompatibility and environmental friendliness with efficient and stable photoluminescence (PL) in the visible spectrum [4,5]. Thanks to such properties, their application in several technological fields, such as bioimaging, sensors, solar energy conversion and in the fabrication of optoelectronic devices is attracting increasing attention in the scientific community [6–9].

The high interest for such nanoparticles is also largely determined by the possibility of synthesizing them via simple bottom-up approaches, producing large quantities of CDs in a single one-pot procedure, starting from low-cost raw carbon sources [4,10,11]. In a typical bottom-up synthesis, opportunely selected organic molecules undergo pyrolysis and polycondensation reactions during high temperature thermal treatments. Then, fluorescent carbon nanoparticles can be isolated as products of the carbonization. The preparations are mainly carried out in hydrothermal/solvothermal conditions, although other carbonization methods are also applied, such as microwave-assisted synthesis and direct pyrolysis from solid state or organic molecular precursors [4,5,10,11].

Among the organic molecules tested as precursors for CDs, some recent works have focused on the use of aromatic compounds featuring two or three hydroxyl functionalities [12–22]. Indeed, such precursors can lead, via polycondensation, to the formation of planar polycyclic aromatic compounds with different configurations, which exhibit an intense fluorescence, high photoluminescence quantum yield (PLQY) and unusually narrow emission bands.

In particular, Yuan et al. [12] employed 1,3,5-trihydroxybenzene (phloroglucinol) as carbon precursor for CDs in a solvothermal synthetic approach. Due to the symmetry of the selected molecule, the resulting CDs are characterized by polyaromatic layers of triangular shape, with very narrow bandwidth emission. Moreover, by properly adjusting the reaction time and/or employing an acid catalyst (H_2SO_4), the CD emission can be tuned across the visible spectrum, by controlling the number of fused benzene ring in the graphenic CDs. Subsequently, it was demonstrated that 1,3-dihydroxybenzene (resorcinol) is more suitable to produce CDs with emission at wavelengths > 600 nm. Such a characteristics was ascribed to the lower activation energy in the polycondensation of resorcinol molecules with respect to that of phloroglucinol [13]. In successive works, o-, m-, p-hydroxybenzene and phloroglucinol were used to synthesize CDs using solvothermal or microwave-assisted approaches [15–21].

Very recently, CDs synthesized from hydroxybenzenes treated at high temperatures (180 – 190°C) in glycols have also been obtained under air atmosphere and ambient pressure [14,22]. The motivation behind the use of such strategy is to promote evaporation and hence removal of H_2O molecules, that form as secondary products of condensation reactions. In such methods, carbonization is performed in open reaction vessels, so to let the water evaporate from the reaction solution. Since H_2O is a reaction side-product, its removal from the reaction environment leads to an increase of the condensation reaction rate [23,24], thus promoting a faster carbonization.

However, in the very limited number of papers reporting such a synthetic strategy [14,22], the whole potential of CD preparation in an open vessel by using high boiling solvents and, especially, the correlation between the employed reaction conditions (e.g. temperature, time, catalysts) and the properties of the obtained CDs have been so far only partially investigated. Understanding how fluorescent polyaromatic species (PAHs) form under such synthetic conditions and how their emission properties evolve during the reaction time can significantly support the rational design of CDs with defined optical properties.

In this work we investigated in depth the mechanisms of hydroxybenzene polycondensation reactions, leading to fluorescent PAHs. In particular, starting from the findings of Yuan et al. [13], we selected resorcinol as hydroxybenzene precursors and EG as solvent.

We monitored the evolution of the spectroscopic properties of the reaction mixture during the synthesis, focusing on how the resorcinol polycondensation results in the formation of fluorescent PAHs. Such a study was facilitated by the use of a non-sealed synthetic apparatus, promptly accessible for sampling anytime during the reaction, unlike the closed solvothermal or microwave reactors. Then, after a purification step needed to remove residual free molecular species, the spectroscopic features of CDs were thoroughly investigated, analyzing their underlying mechanisms. In particular, thanks to a convenient integration of steady-state and time-resolved fluorescence experiments, two distinct contributions were assigned to the CD emission, deriving from (i) PAH and (ii) CD surface states.

Moreover, in order to increase the rate of resorcinol polycondensation and carbonization, the effect of catalysts in assisting the reaction was investigated. Firstly, NaOH was tested as basic catalyst. In fact, NaOH has been previously used as dehydration and carbonization promoter in some bottom-up CDs synthetic approaches [25] and, considering the resorcinol reactivity in the presence of OH^- [26,27], it is expected to be effective in activating its condensation reactions. In addition, we investigated the effect of an acidic catalyst, H_2SO_4, previously used in solvothermal CD synthesis [12].

Another crucial aspect in the optical performance of CDs is their resistance to photochemical degradation. In fact, poor photobleaching resistance may pose severe limitations to the applications of CDs in many technological fields [28]. Nevertheless, the photostability of CDs synthesized from resorcinol or other hydroxybenzenes is currently largely unexplored. Moreover, as reported in previous works [29–32], elucidating the mechanisms behind the photodegradation of PL features has been found useful to clarify the debated origin of CD PL. In particular, it has made possible to distinguish surface site emission from that deriving from molecular fluorophores formed during the CD synthesis. Therefore, we investigated the spectroscopic properties of CDs under exposure to continuous UV irradiation and showed that the two CD emission bands exhibit a different resistance to photochemical degradation, thus confirming their origin from either CD' surface energy state emission or PAH fluorescence.

Finally, we demonstrated a relevant quenching/enhancing effect of the CD emission in the presence of acidic or basic compounds in their surrounding environment, feature that makes such CDs interesting candidates for on/off sensing or stimulus-responsive devices.

2. Experimental section

2.1 Chemicals

Resorcinol (≥ 99%), ethylene glycol (EG, ≥ 99%), sodium hydroxide (NaOH, ≥ 97%), hydrochloric acid (HCl, 37%), sulphuric acid (H_2SO_4, 95.0 – 98.0%), ethanol (EtOH, ≥ 99.5%,) were purchased by Sigma Aldrich and used as received, without any further purification or distillation. Solvents were of analytical grade. All aqueous solutions were prepared using MilliQ water.

2.2 Synthesis of CDs

CDs synthesized without added catalysts (n-CDs) were prepared through thermal-assisted carbonization of resorcinol in a high boiling polar solvent (EG). First, EG (12 mL) was heated at 180 °C in a round bottom flask. Then, a solution of resorcinol (1.5 g) in EG (3 mL) was quickly injected through a syringe, and the system was allowed to react at 180°C for 6 h. The vessel was kept open throughout the reaction in order to promote evaporation of water deriving from resorcinol polycondensations. Moreover, the reaction temperature was monitored and kept constant via a temperature controller connected to a heating mantle by a thermocouple placed inside the reaction flask. For CDs synthesized with base catalyst (b-CDs) and acid catalyst (a-CDs), soon after the injection of the resorcinol solution, 500 μL of a 2 M aqueous solution of either NaOH or H_2SO_4 were quickly injected into the reaction vessel, corresponding to 1 mmol of added catalyst.

2.3 Purification of CDs

The obtained n-CDs, b-CDs and a-CDs were purified by washing with a very diluted (~ 10^{-4} M) HCl aqueous solution. In details, 2 mL of raw reaction batch were mixed with 5 mL of HCl solution under vigorous stirring. Then, such solution was centrifuged (at 9000 rpm for 30 min), and a dark brown precipitate was obtained. The solid precipitate was further dispersed in water and centrifuged, repeating the same procedure 4 times. At the end of the purification, the dark precipitate was dried under vacuum and then weighted to calculate the mass reaction yield. The as-obtained CDs in the form of dry brown powder were dispersed in ethanol for further analysis.

2.4 Morphological investigation

Transmission Electron Microscopy (TEM) analysis was carried out using a JEOL JEM1011 microscope, equipped with a W filament operating at 100 kV. The images were acquired using an Olympus Quemesa CCD camera. The samples were prepared by dipping carbon-coated copper grids in opportunely diluted ethanol solutions of CDs, then leaving the grids to dry in air. The statistical analysis on CD size was performed by using a free image analysis software (ImageJ, v.1.52a).

2.5 WAXS analysis

Drops of CD solutions were deposited on miscut silicon substrates. Wide Angle X-ray Scattering (WAXS) data were collected in grazing incidence reflection geometry (GIWAXS) at the X-ray MicroImaging Laboratory (XMI-L@b), equipped with a Fr-E+ SuperBright rotating anode table-top microsource (Cu Kα, λ = 0.15405 nm, 2475W), a multilayer focusing optics (Confocal Max-Flux; CMF 15-105) and a three-pinholes camera (Rigaku SMAX-3000).

An image plate detector with 100 μm pixel size was employed, placed at 87 mm from the sample. The grazing incidence angle was 0.2°. GIWAXS data were calibrated by using Ag behenate powder as reference material.

2.6 Infrared Spectroscopy analysis

Fourier-Transform Infrared (FT-IR) investigation was carried out using a PerkinElmer Spectrum One Fourier Transform Infrared spectrometer. All spectra were recorded using the attenuated total reflection technique, with a 4 mm diameter diamond microprism as internal reflection element. Approximately 5 μL of CD ethanol dispersions (2 mg/mL) were drop-casted onto the surface of the microprism and the solvent was allowed to evaporate. Spectra were then acquired on CD powders. In order to investigate the spectroscopic changes upon addition of strong acid and bases, respectively 1 mmol of HCl and NaOH (from 2M aqueous solutions) were added to the aforementioned CD dispersions; subsequent drop-casting procedure and spectrum acquisition conditions were kept unchanged.

2.7 UV-Vis Spectroscopic investigation

UV-Vis absorption spectra were recorded with a Cary 5000 (Agilent Technologies, Inc., Santa Clara, CA, USA) UV-Vis-NIR spectrophotometer. Steady-state PL emission spectra were acquired using a Fluorolog 3 spectrofluorometer (HORIBA Jobin-Yvon GmbH, Bensheim, Germany), equipped with double-grating excitation and emission monochromators and a 450W Xe lamp as excitation light source. The time evolution of the spectroscopic properties during the synthesis was investigated by drawing small aliquots (~ 100 μL) from the reaction mixture, diluting them in ethanol and recording UV-Vis absorption, PL excitation and emission spectra. PL emission spectra were recorded using excitation wavelengths (λ_{exc}) at 350 and 485 nm, while PL excitation spectra were recorded at the emission wavelength (λ_{em}) of 565 nm. To prevent re-absorption of emitted photons, sample solutions were diluted to have the absorbance at the excitation wavelength ≤ 0.1 a.u. Absolute PLQY was measured using a "Quanta-phi" integration sphere coated with Spectralon® (HORIBA Jobin Yvon GmbH, Bensheim, Germany) (reflectance ≥95% in the range 250–2500 nm). Time-Resolved PL (TRPL) measurements were carried out by Time Correlated Single Photon Counting (TCSPC) technique, with a FluoroHub (HORIBA Jobin-Yvon). CDs solutions were excited using 80 picosecond laser diode sources at 375 nm (NanoLED 375L) and at 485 nm (NanoLED 485L). Time resolution was ~300 ps for all the measurements.

2.8 UV irradiation experiment

Ethanol dispersions of CDs (0.03 mg/mL) were placed in quartz cuvettes and exposed to a medium pressure Hg lamp (λ > 250 nm) under continuous magnetic stirring. In particular, samples were irradiated with a light beam perpendicular to the cuvette face with a section able to cover the entire volume of CD dispersion; the irradiance of such beam was 0.07 W/cm^2. Periodically, the cuvettes were transferred to the UV-Vis spectrophotometer and spectrofluorometer for spectroscopic monitoring.

2.9 Computational Methods

The structure of several possible PAHs with OH functionalization was optimized with quantum mechanics calculation by means of the Gaussian 16 suite [33]. The level of theory was set within the DFT framework with the B3LYP hybrid functional and the 6-311 ++ G(d,p) basis

set [34–36]. The interaction of computed structures with solvent water was accounted for by applying the Self Consistent Reaction Field (SCRF) approach and simulating the dielectric solvent through the Polarizable Continuum Model (PCM) calculation within the integral equation formalism (IEFPCM) [37,38]. Frequency calculations were performed on the optimized structures at the same theory level, and no imaginary frequencies were found, confirming their character of energy minima. Ball and stick representation of the structures was performed with the Gaussian package. The calculated absorbance spectra were simulated by assuming convolution of gaussian bands centered at the computed transitions, with height proportional to the oscillator strength and half width at half height of 0.333 eV.

3. Results and discussion

3.1 Synthesis of n-CDs and formation of fluorescent PAHs

n-CDs are obtained through a thermal synthetic approach in an open reaction vessel, followed by simple and solvent-saving purification steps. This method allows to easily monitor variations of spectroscopic properties during the reaction, taking advantage of the open reactor. In particular, our attention is focused on polycondensations between resorcinol molecules, which lead to fluorescent PAHs.

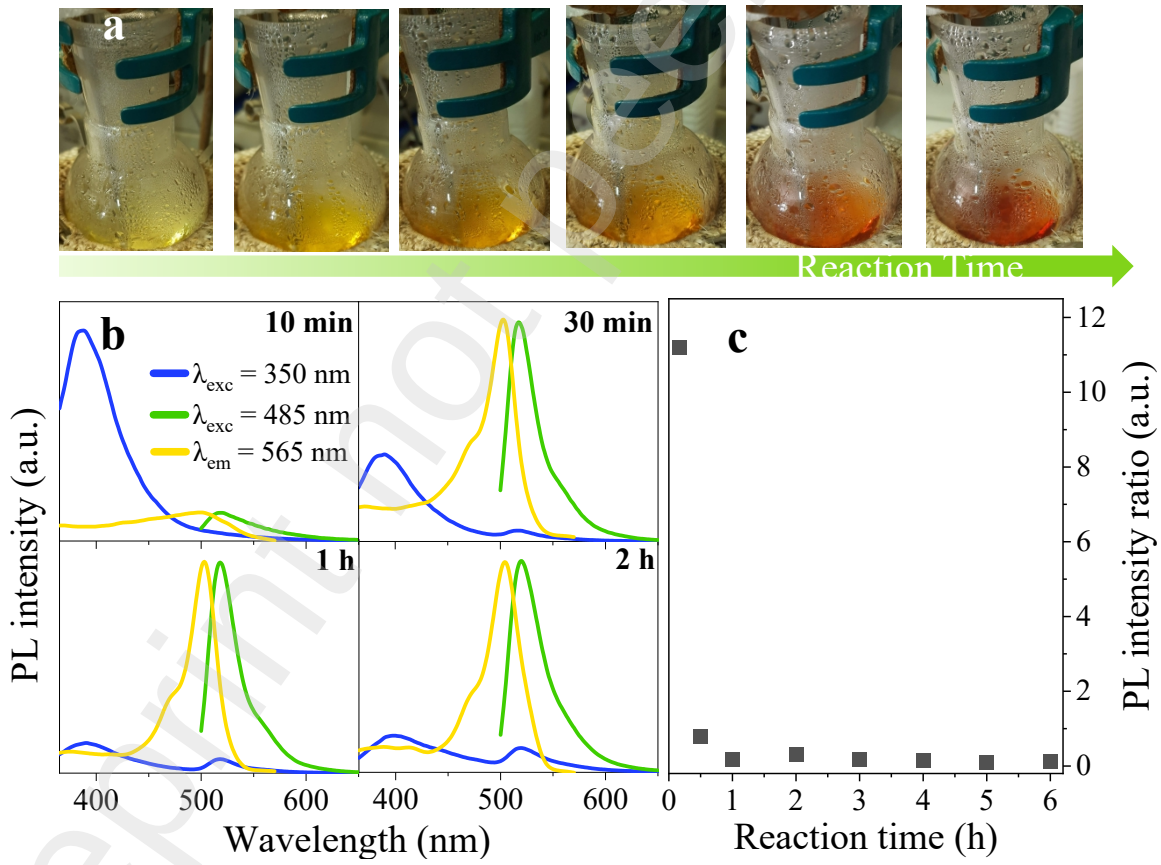

Figure 1: (a) Pictures of the reaction vessel during the synthesis of n-CDs, recorded (from left to right) at 10, 30, 45, 60, 180 and 300 min reaction time (b) PL spectra (λ_{exc} of 350nm and 485 nm, blue and green line, respectively) and PL excitation spectra (λ_{em} = 565 nm, yellow line), recorded during the synthesis at 10 min, 30 min, 1 h and 2 h reaction time (c) ratio between the intensity of the PL band at 400 nm (λ_{exc} = 350 nm) and at 520 nm (λ_{exc} = 485 nm) as a function of reaction time.

Figure 1Figure 1a reports the pictures of the reactor vessel at increasing reaction time. The initially colorless EG turns to pale yellow 10 min after the addition of resorcinol and then the color shifts to orange/red. Such color changes can be associated to the formation, and gradual increase in concentration, of PAHs from resorcinol polycondensations, and eventually n-CDs, with optical absorption in the visible region.

Resorcinol solution at the beginning of reaction does not show any fluorescence, while exhibits an absorption band in the UV, centered at 276 nm (Figure S1a). PL excitation and emission spectra, recorded on the raw reaction batch at different reaction times (from10 min to 2 h), are reported in Figure 1b. When excited at 350 nm (blue curves), the PL spectra display two bands peaked at 400 nm and at 520 nm, with relative intensity changing with reaction time. When λ_{exc} is set at 485 nm, it is possible to excite only the emission band centered at 520 nm, which is characterized by a narrow line shape that recalls the emission of a molecular fluorophore. Similarly, the profiles of the PL excitation spectra are characterized by a narrow band that approximately mirrors the green emission band. Instead, the emission band centered at 400 nm (i.e. blue region) is very broad (FWHM ~ 60 nm) and asymmetric and hence ascribable to a heterogeneous ensemble of emitting species, rather than to a single fluorophore.

In Figure 1c the intensity ratio of the two emission bands as a function of the reaction time is reported. At reaction times longer than 10 min, the ratio decreases sharply, reaching a plateau after 1h. This evidence points out that the blue emission, very intense at the early stages of reaction, is strongly quenched in time, due to emitting species that are consumed or modified within the first hour of reaction.

The blue emitting fluorophores reasonably form at very short reaction times through the condensation of two or more resorcinol molecules (Scheme 1) that are thermally activated (being the system heated at 180°C) and favored by the specific chemical reactivity of resorcinol [26] (Figure S1b). In particular, from the condensation of 3-4 resorcinol molecules, small–OH terminated PAHs should form. Such small PAHs have been already reported to exhibit blue fluorescence [39–43]. Therefore, the intense blue emission observed at short reaction times can be safely ascribed to the early formation of these species. On the other hand, EG is expected not to participate to the polycondensations leading to PAHs, due to its much lower reactivity [44]. At increased reaction time, the small PAHs are progressively consumed in part to favor the formation, by the addition of more aromatic rings, of larger PAHs emitting in the green region. Indeed, sharp bands with spectrally resolved vibronic transitions, as the green emission observed in Figure 1b, closely evoke the UV-Vis spectroscopic characteristics of either PAHs or molecular dyes based on polycyclic aromatic units. After their formation, PAHs can be found dispersed in solution, bound to CD surface or even incorporated into their carbonaceous core, thus acting as emitting centers for n-CDs [39–41,45–47]. However, a weaker blue emission stays, almost constant in intensity, also at longer reaction times.

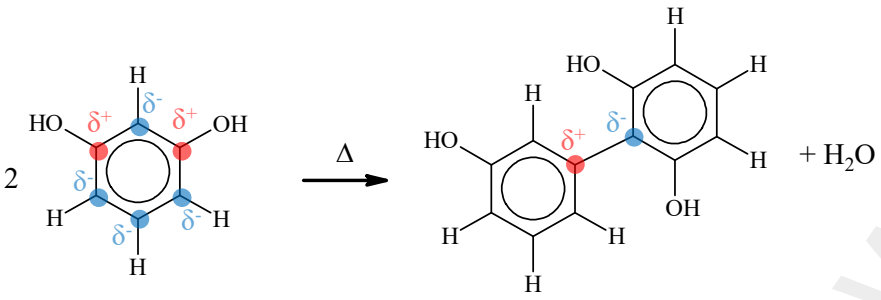

Scheme 1: Thermally activated condensation of resorcinol molecules.

3.2 Modelling of –OH terminated PAHs chemical structure and spectroscopic properties

In order to assess the proposed reaction mechanism, the formation and time evolution of polyaromatic fluorescent molecules during the reaction was further studied performing a DFT theoretical investigation. In particular, possible alterations in the structural properties of PAHs occurring during the reaction (i.e. variation of number and/or arrangement of aromatic rings, –OH groups, molecular planarity) were investigated, to understand whether and how such modifications may affect the energy level structure of the PAHs, and, accordingly, their spectroscopic properties.

A variety of PAH structures were optimized featuring increasing number of benzenoid rings and approximately one –OH substituent for each ring at the edge of the structure. In general, when a structure with a certain number of rings is considered, –OH groups can be found in different amounts and positions, depending on how resorcinol molecules assemble via condensation. Moreover, the geometrical arrangement of the benzenoid rings can also vary, according to the relative orientation of the condensed resorcinol molecules. Either ring arrangement, number or position of –OH may influence the optical features of PAHs.

The DFT calculated UV-vis absorption spectra of –OH terminated PAHs with 1 – 4 rings are reported in Figure 2, with the representation of each structure in the inset. The resorcinol single unit shows two absorption bands in the UV, with the transition from the Highest Occupied Molecular Orbital (HOMO) to the Lowest Unoccupied Molecular Orbital (LUMO) at about 250 nm. This band can be correlated to the absorption band experimentally measured for resorcinol solution in ethanol, that has a maximum at 276 nm (Figure S1a). The fusion of two rings (Figure 2b) induces the HOMO-LUMO (HL) gap to redshift, while the increase of the number of fused rings to 3 and 4 (Figure 2c,d) leads to a further progressive redshift of the HL gap. In general, the same trend is also observed for larger PAHs with 7 – 9 rings (Figure S2). Indeed, such a behaviour is in agreement with the HL gap redshift observed in PAHs as the number of benzene rings increases [48].

However, the presence of –OH substituents at the edges of the investigated structures, also affects the observed optical features. In particular, terminal –OH groups are generally found to further reduce the HL gap, compared to the correspondent unsubstituted PAHs. For example, the structure shown in Figure 2d can be regarded as pyrene (a paradigmatic PAH system) with the substitution of four edge H atoms with likewise –OH groups. The presence of –OH substituents induces a narrowing HL gap of ~200 meV, being the exact value dependent on the relative position of –OH functionalities, with respect to unsubstituted pyrene. In addition, the –OH groups affect the oscillator strength of the HL transition, although with a stronger dependence on the relative position of the –OH groups. For example, considering the –OH

functionalized 7-ring coronene (Figure S2a), the HL gap is redshifted with respect to the analogously functionalized pyrene (Figure 2d), however with a decrease of the HL oscillator strength. The trend is exemplified in the case of the pyrene system, where the narrowing of the HL gap by increasing the number of terminal –OH groups is paired with the decrease of the oscillator strength (Figure S3). However, large redshifts paired with very high oscillator strength values were also observed, in particular for 8-rings and 9-rings structures in Figure S2b-d. This suggests that PAHs with both redshifted and intense optical transitions can be formed as products of resorcinol condensations and thus can be considered responsible for the strong green emission band of synthesized CDs.

Lastly, planarity of PAHs is a crucial aspect. In fact, all structures considered above have a planar geometry. However, planarity is not to be taken for granted when very large PAHs are considered, as it is also largely affected by the specific rings' assembly and the relative position of their –OH substituents. Indeed, considering the 12-rings PAHs in Figure S4a-c, the HL gap is remarkably larger than that found for the 8 or 9 ring PAHs (Figure S2b-d). Such an opposite trend can be assigned to the non-planarity of the structure. However, by changing the ring organization in order to obtain a planar geometry with the same number of rings and –OH groups (Figure S4d), the HL gap is found to redshift, thus confirming the role of planarity, alongside the number of benzenoid rings, in inducing a redshift.

Despite the difficulty in directly comparing the quantum mechanical calculations with the experimental data — due to the complexity of the system — these results still provide useful insights for the elucidation of the shift of the PAHs emission from blue to green as the reaction proceeds. Indeed, such a shift can be explained on the basis of the formation of planar –OH terminated PAHs with increased number of benzenoid rings. In particular, PAHs with a defined number and position of terminal –OH groups and a suitable arrangement of benzenoid rings display a redshifted emission as well as high oscillator strength, which can account for the intense green fluorescence of CDs, as observed during their synthesis. On the other hand, experimentally, the HL gap is not found to further shift from the green to the red region at increasing reaction time. The performed calculations highlighted that for polyaromatic structures consisting of several benzenoid rings, geometrical arrangements characterized by distorted and non-planar structure are possible. Notably, these structures show absorption transitions shifted towards higher energies, as a consequence of interruption of extended conjugation in the molecule. Consequently, when several (e.g. >10) benzenoid rings are condensed in a PAH, the probability of forming a distorted molecule can be reasonably assumed to increase, thus explaining the occurrence of structures with larger HL gaps.

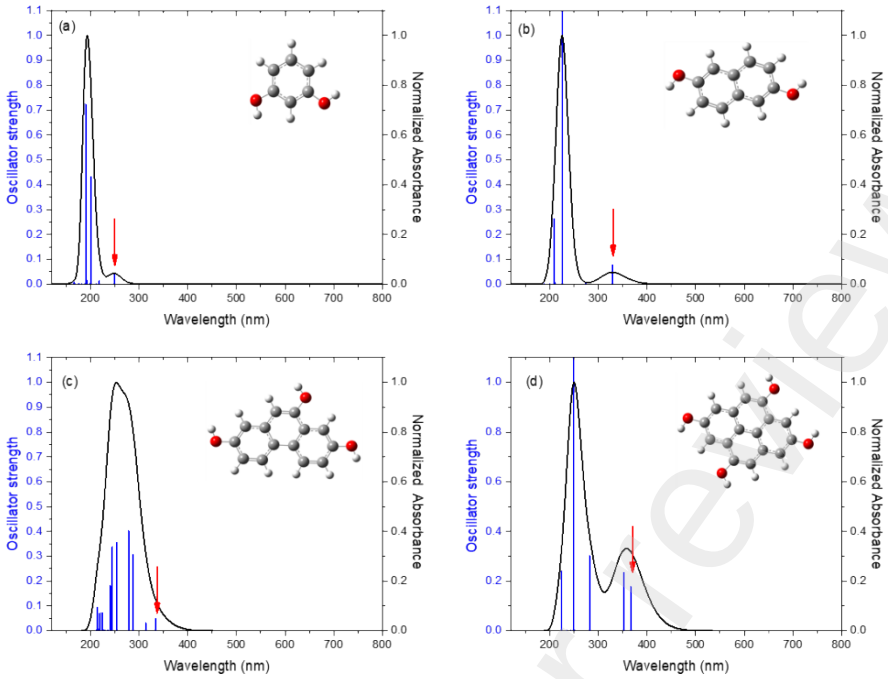

Figure 2: Simulated absorption spectra and calculated oscillator strength of (a) 1-ring, (b) 2-rings, (c) 3-rings and (d) 4-rings structures. The insets report the representation of each structure (C atom = grey sphere, H atom = white sphere, O atom = red sphere).

3.3 n-CDs: morphology, structure and optical properties

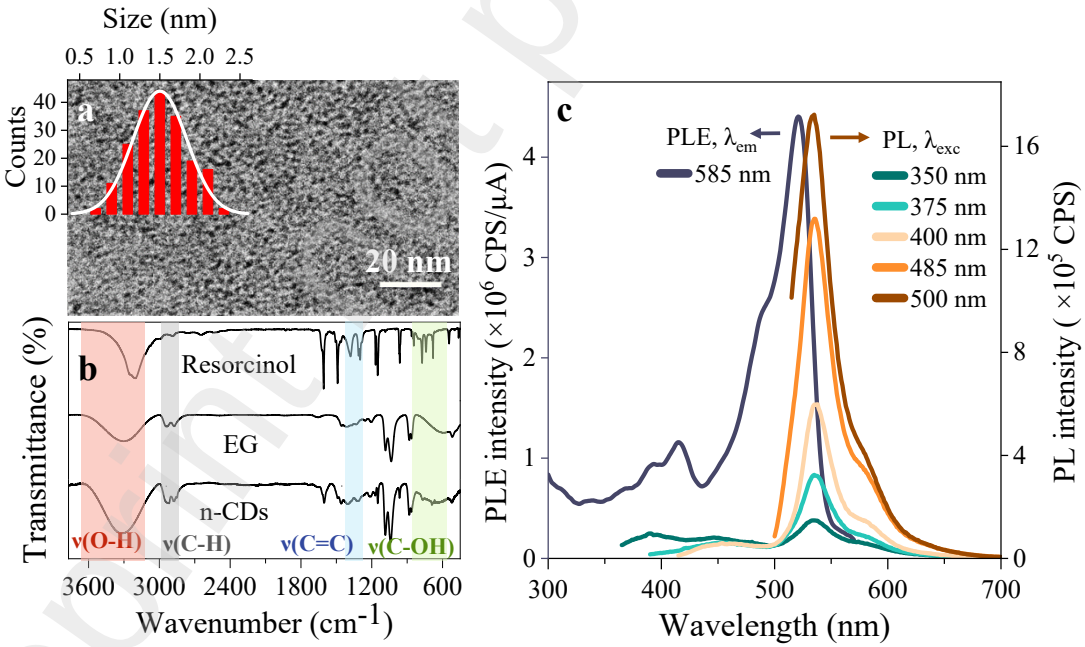

Figure 3: (a) TEM micrograph and size distribution histogram (inset) of the purified n-CDs; (b) FT-IR spectrum of the n-CDs compared with the spectra of resorcinol and ethylene glycol; (c) PL excitation (λ_{em} = 585 nm black line) and emission spectra at different excitation wavelengths of purified n-CDs dispersed in ethanol.

The purification procedure described in the Experimental Section was found effective in removing unreacted resorcinol and molecular reaction intermediates not bound to the CD

surface; this can be confirmed by the UV-Vis absorption investigation of purified n-CDs (Figure S5**Error! Reference source not found.**), which highlights a dampening of the characteristic resorcinol absorption band at 276 nm after the precipitation and redispersion cycles.

After purification, n-CDs have been morphologically characterized by TEM. The micrograph (Figure 3a) shows spheroidal shaped nanoparticles with a mean size of 1.5 nm (σ = 20%).

GIWAXS 2D pattern was collected on n-CDs deposited onto Si substrate (Figure S6a), and after calibration and centering was transformed in the GIWAXS 1D profile shown in Figure S6b. Upon data indexing [49], the identification of a crystalline phase corresponding to a carbon phase was possible [50]. The very broad peaks centered at ~8° and ~22° (Figure S6b), indicate an overall lower degree of crystallinity with respect to CDs synthesized either from resorcinol or phloroglucinol via solvothermal approaches, where high pressure are reached due to the confined reaction environment [12,13]. The poor crystallinity of these CDs can be correlated to the occurrence of the distorted polyaromatic structures, which would be consistent with the formation of the large and non-planar –OH terminated PAHs resulting from DFT investigation (Sec.3.2).

Figure 3b shows a comparison between the FT-IR spectrum of n-CDs, resorcinol and the solvent, EG. A detailed list reporting the assignment of each peak in the spectra is provided in Table S1 and Figure S7. The most relevant features observed in the spectrum of n-CDs are a broad band centered at 3320 cm^{-1} ascribed to the stretching vibrations of the O-H bond, a doublet at 2950 and 2880 cm^{-1}, assigned to C-H stretching vibration, a peak at 1603 cm^{-1} due to aromatic C=C within the carbogenic core, along with various peaks in the region 960-1150 cm^{-1} related to the stretching of C-O bonds. In particular, these C-O stretching peaks are also present in the spectrum of resorcinol. On the other hand, the doublets at 2950 and 2880 cm^{-1} and at 1085 and 1040 cm^{-1} are also found in the spectrum of EG. Since no carbonyl nor carboxyl features are observed in the FT-IR spectrum of n-CDs, it can be inferred that the surface of such nanoparticles is crowded by –OH groups. Moreover, the ethylene glycol characteristic C–O and C–H stretching peaks in the spectrum of CDs distinctly indicate the presence of such molecule in the purified sample. Due to the chemical affinity of diol molecules for the –OH surface chemical groups of CDs and the capability of both species to form hydrogen bonds, it is very likely that some residual EG molecules remain at the surface of n-CDs, bound to the–OH groups.

A ζ-potential of ~ -25 mV was measured for n-CDs, indicating a negatively charged surface for the purified nanoparticles, likely ascribed to deprotonated –OH or $C–O^-$ groups at the n-CDs surface. Notably, since the surface of n-CDs is not expected to feature long chain molecules/moieties that may enable a steric stabilization, their negative charge has to be considered essential for their colloidal stability.

PL excitation and emission spectra of purified n-CDs, recorded at several λ_{exc} in the range between 350 and 500 nm are reported in Figure 3c. In the PL excitation spectrum, narrow bands centered at 520 nm and 415 nm are observed, together with weaker shoulders at 490 nm and 390 nm. The PL emission spectra show a very narrow band peaked at 535 nm with a full width at half maximum (FWHM) of only ~36 nm, accompanied by a weaker shoulder at 585 nm, independent from λ_{exc}. The absolute PLQY of such green band is of ~ 42%, when excited at 485 nm (Table 2).

Narrow bandwidth excitation and emission optical bands in the visible region of the spectrum have been reported in some previous works in which bottom-up synthesis of CDs using either resorcinol or other benzenediols or benzenetriols was examined [12–21]. In some reports, the small FWHM values result from the intrinsic emission from the CD carbogenic core states or from HOMO-LUMO transitions of graphenic layers constituting the conjugated sp^2 domains in the core of CDs [12,13,16–20]. However, here, n-CDs display a less marked structural order. Nonetheless their optical properties are still characterized by sharp excitation and emission bands that can only be explained based on the presence of fluorescent PAHs in the nanoparticles. In particular, since in n-CDs the contribution of free molecular fluorophores in solution is eliminated through purification, the remaining PAHs responsible for the green luminescence could be either enclosed within the carbogenic matrix of the n-CDs or bound externally onto their surface.

Furthermore, the already weak blue emission observed for non-purified n-CDs at long reaction times (Figure 1b), is even weaker for purified n-CDs (Figure 3c). Such an intensity dampening can be ascribed to removal of free small PAHs present in the raw reaction batch. In addition, in purified n-CDs a very weak and broad emission found between 365 and 500 nm can be observed only for λ_{exc} up to 400 nm and characterized by an excitation wavelength dependence. Since such blue band can no more be ascribed to small PAHs, it can be tentatively attributed to the radiative emission from surface states of n-CDs [11,51–55]. Finally, the green band of the purified sample is slightly redshifted with respect to that observed in non-purified n-CDs (Figure 1b). This shift is due to a solvatochromic effect induced by a polarity variation of the surrounding environment. In fact, the spectra in Figure 1b are recorded in the presence of EG, which will be only later removed upon purification (Figure 3c). Thus EG, by increasing the polarity, can be considered responsible of the observed shift, in agreement with the behavior reported by T. Yoshinaga et al. for CDs synthesized from phloroglucinol in a glycol solvent [18].

Therefore, consistently with the discussed attributions, the spectroscopic features of n-CDs can be rationalized and summarized as follows (Figure 4).

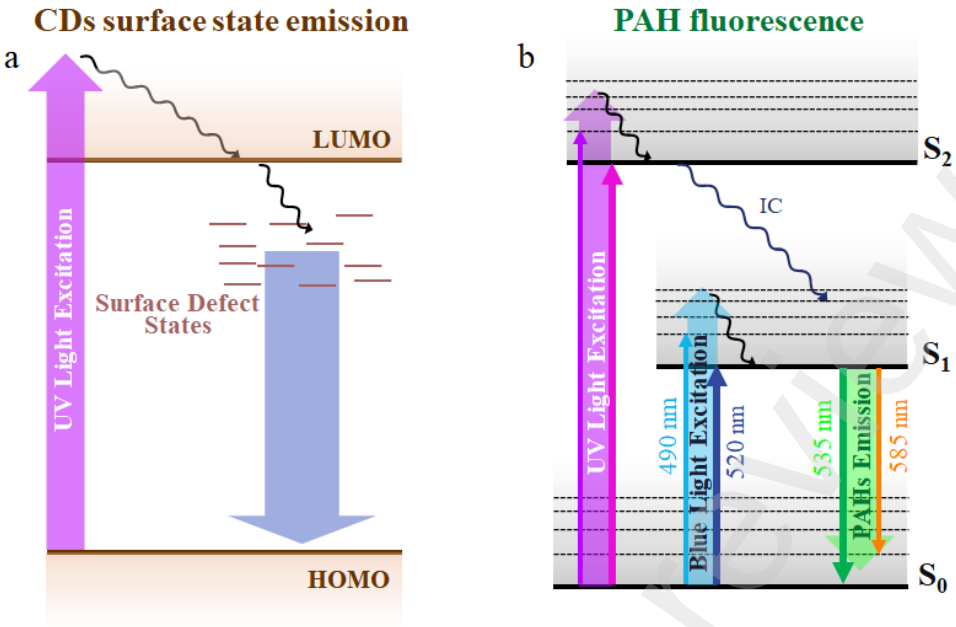

Figure 4: Schematic description of the proposed mechanisms explaining the spectroscopic features of n-CDs; the CDs' levels and the PAHs' levels are represented on different arbitrary energy scales.

Firstly, the PAHs emission originates from the radiative decay of two electronically excited states (S_2 and S_1) towards the ground state (S_0). Such transitions correspond to the PL excitation bands at 390 – 415 nm ($S_0 \rightarrow S_2$) and at 490 – 520 nm ($S_0 \rightarrow S_1$). According to the literature, the strong absorption of n-CDs in the UV (Figure S5) is ascribed to transitions between states, due to planar or non-planar conjugated C=C double bond structures in the carbogenic core of CDs [56–58]. Upon excitation with UV light (at 350 – 375 nm), photons can be absorbed either by the CD carbogenic core (Figure 4a), or by PAHs through a $S_0 \rightarrow S_2$ absorption transition (Figure 4b). Then, radiative recombination can occur from CD surface states after a non-radiative excited state energy transfer from the LUMO of CD core states. Surface state recombination accounts for the excitation dependent blue band of n-CDs. On the other hand, UV excitation of PAHs results in the narrow emission bands found at 535 and 585 nm after an intersystem crossing from S_2 to S_1, according to Kasha's rule [59]. Similarly, when excited at 485 nm, radiative decay in PAHs directly occurs with a S1 → S0 transition (Figure 4b).

To assess these attributions, we investigated the TRPL decays of n-CDs in correspondence of the two emission bands (Figure 5a,b), exciting in the UV (at 375 nm) and in the blue (at 485 nm).

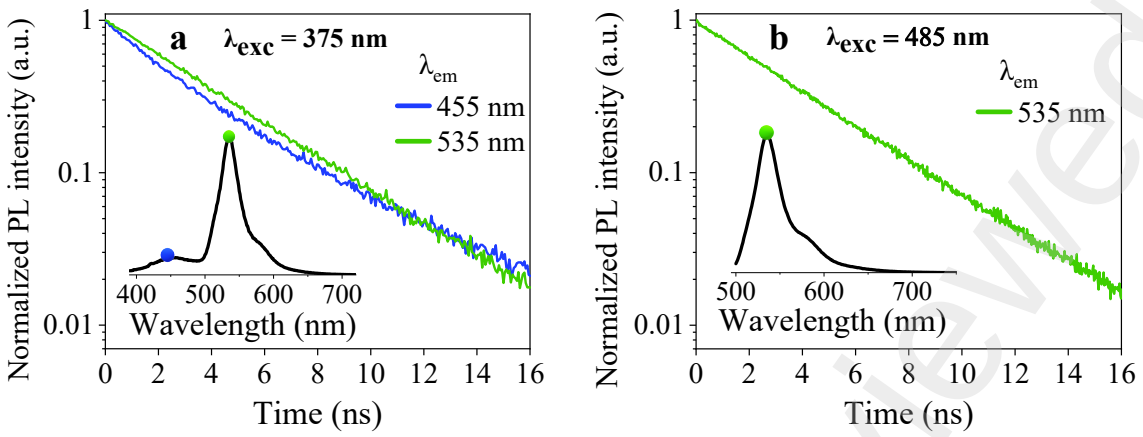

Figure 5: TRPL decays of CDs excited at (a) 375 nm and (b) 485 nm. The insets show the steady-state PL spectra excited at the corresponding excitation wavelengths; the PL intensity decays have been monitored in correspondence of the emission peaks, i.e. at 455 and 535 nm for λ_{exc} = 375 nm and at 535 for λ_{exc} = 485 nm.

The TRPL decays at 535 nm show the same slope, independently from the λ_{exc}, while a slight difference is observed in the decay of the blue band emitting at 455 nm. The decay of the green band can be fitted with a mono-exponential function, yielding a lifetime of (3.9± 0.3) ns. On the other hand, for fitting the decay of the blue band, an additional stretched component with a lifetime of (1.8 ± 0.5) ns was required (details about the fitting procedure are provided in the Supplementary Information). The mono-exponential decay of the PL at 535 nm is compatible with a radiative decay arising from molecular fluorophores, such as PAHs, in agreement with its attribution [60,61]. Conversely, the stretched PL decay at 455 nm denotes the occurrence of recombination pathways originating from a heterogeneous ensemble of emitting centers, further proving that emission in the blue region has to be associated with radiative recombinations occurring at the surface energy states of n-CDs.

3.4 Synthesis of b-CDs and a-CDs

The study of n-CDs synthetic reaction allows to infer that the carbonization step which leads to nanoparticle formation is a rather slow and low yield process. In fact, after a reaction time of 6 h only a small number of purified n-CDs can be obtained (< 0.7% of the initial resorcinol mass). Therefore, very long reaction times are needed for the complete consumption of precursor, which in turn makes the yield of the synthesis very low and thus not efficient for up-scaled the CD production process. In order to speed up the reaction, two types of catalysts have been tested, namely NaOH and H_2SO_4, following the procedures reported in the Experimental Section. Both the basic and the acid catalysts are expected to promote resorcinol condensation reactions, through different mechanisms (Scheme 2). In particular, when reacting with resorcinol, OH^- deriving from the base catalyst should form resorcinol monoanion (phenolate), which has enhanced reactivity with respect to resorcinol due to electron delocalization to adjacent carbon atoms [26,27,62] (Scheme 2a). On the other hand, H^+ deriving from the acid catalyst promotes the formation of the leaving group (H_2O) during the condensation, by protonation of a resorcinol hydroxyl group [26,62,63] (Scheme 2b).

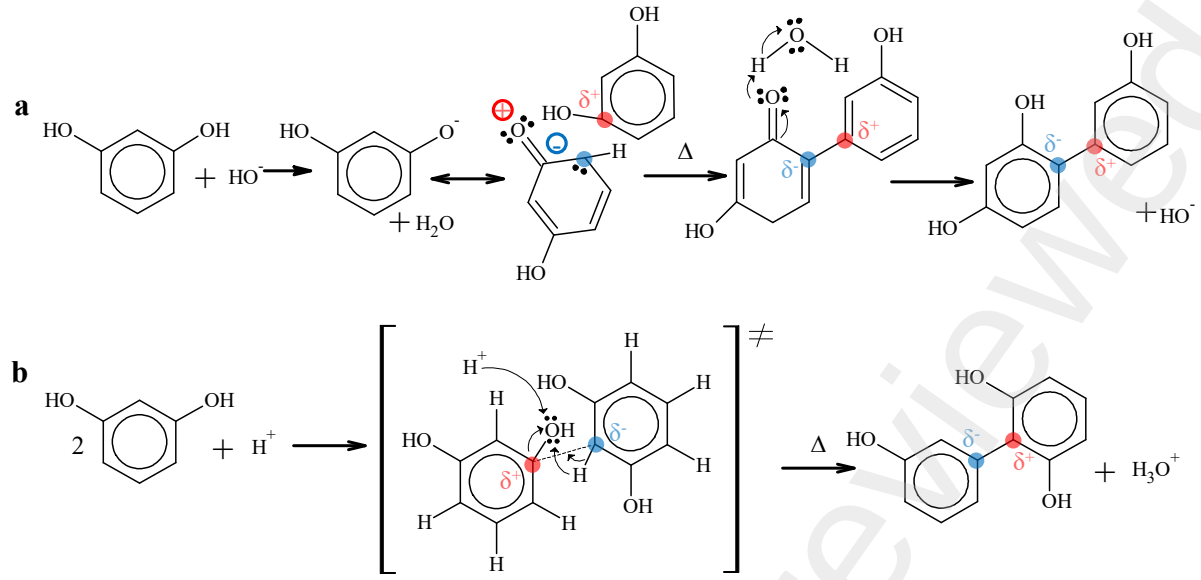

Scheme 2: Different mechanisms for (a) base (NaOH) and (b) acid (H_2SO_4) catalyzed condensation of resorcinol molecules.

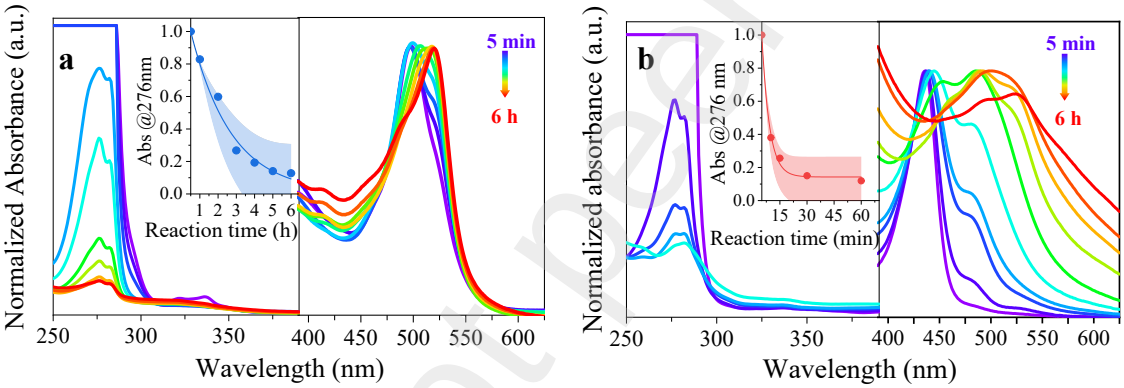

Figure 6: Comparison of the UV (left panels) and visible (right panels) absorption spectra recorded at increasing reaction times up to 6 h for (a) b-CDs ~~(a)~~ and (b) a-CDs. The insets show the trend of the absorbance at 276 nm (peak of the resorcinol absorption band) as a function of reaction time, with the results of the fitting procedure shown as solid lines alongside its 95% confidence interval.

Since both the base and acid catalyzed mechanisms are expected to promote a faster resorcinol polycondensation, the reaction rate in the presence of the two investigated catalysts has been examined by monitoring the progressive dampening of resorcinol characteristic absorption band at 276 nm (Figure S1a). In the synthesis of b-CDs (Figure 6a), the intensity of absorption band decreases in time and the dampening can be fitted with a mono-exponential function characterized by a decay time of ~2 h (SI, Table S2). The decay reaches a plateau at ~ 6 h, indicating that the resorcinol consumption is almost complete at that reaction time. On the other hand, in the absence of catalysts (with equal concentration of precursor), saturation of absorbance is observed at all investigated reaction times up to 6 h (Figure S8). This indicates that resorcinol concentration remains always very high for n-CDs, i.e. that the reaction kinetics is very slow. Moreover, after the same reaction time (6 h) and post-synthetic treatments, for b-CDs a large increase of the reaction yield is found. In fact, while for n-CDs only a small amount (< 10 mg) of purified product is obtained, for b-CDs around 250 mg are collected, corresponding to a mass reaction yield of 17%.

Interestingly, when H_2SO_4 is added (Figure 6b), an even faster consumption rate of resorcinol is observed, and the absorbance decay reaches a plateau in only 30 min. However, examining the UV-Vis absorption spectra at long wavelength (Figure 6b, right side panel), a contribution due to light scattering that becomes gradually more relevant as the reaction time increases can be observed. This contribution can be ascribed to the formation of large aggregates caused by the poor colloidal stability of a-CDs, which leads to particle coalescence. In fact, ζ-potential measurements of a-CDs indicate a very small positive value (~ + 0.5 mV), in contrast to the high negative ζ-potentials obtained for b-CDs and n-CDs (Table 1). As previously mentioned, considering that the surface of CDs is crowded only by small functional groups ($–CO^-$ and –OH groups), steric stabilization is not possible and only electrostatic repulsion is responsible for the stability of the colloidal dispersion. Thus, the small net surface charge of a-CDs leads to unstable colloidal suspensions, which results into nanoparticle coalescence and formation of large aggregates responsible for the observed light scattering.

Sample	ζ-potential (mV)
n-CDs	- 24.7
b-CDs	- 27.8
a-CDs	+ 0.5

Table 1: ζ-potential measurements performed on the n-CDs, b-CDs- and a-CDs

After purification, the PL spectra of b-CDs and a-CDs (Figure 7) are both characterized by a broad and excitation dependent blue band centered at around 400 nm for λ_{exc} = 350 nm, and a narrow green band independent from excitation peaking at 535 nm, similarly to the emissions of n-CDs (Figure 3c). As discussed in the previous sections, we attribute these two bands respectively to emission from CD surface energy states and from PAHs formed by resorcinol polycondensation reactions. Thus, the presence of catalyst does not affect very much the spectral shape and position of the final molecular PAH conveying the green fluorescence to these CDs.

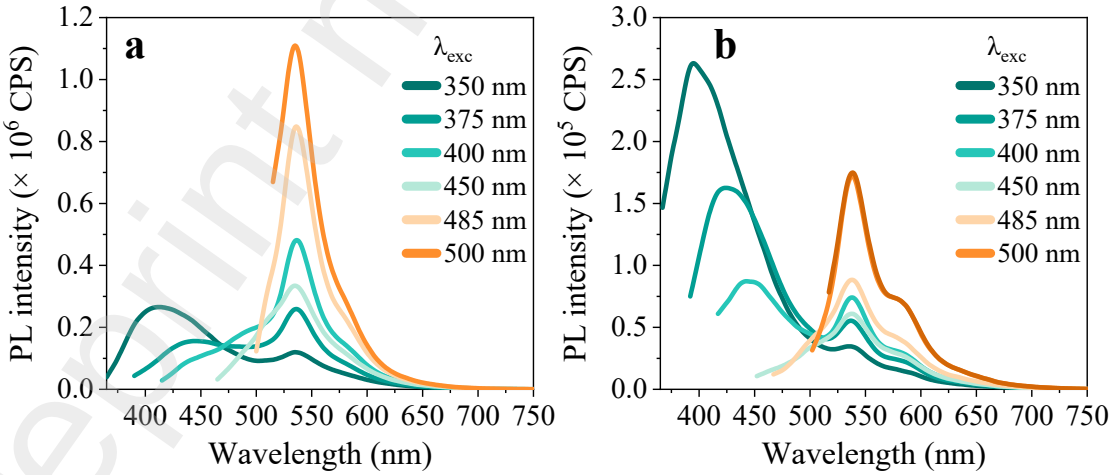

Figure 7: PL spectra at different excitation wavelengths of purified (a) b-CDs and (b) a-CDs obtained at the end of the synthesis.

However, in n-CDs, b-CDs and a-CDs the bands exhibit different relative intensities. In particular, an enhancement of the blue band intensity is observed for b-CDs (Figure 7a) with

respect to n-CDs (Figure 3c); this band becomes even more intense and predominant for a-CDs (Figure 7b) at high energy excitation. Such result can be due to the modification induced by the presence of acid and base catalysts on the surface states responsible for the emission. Furthermore, in the three CDs samples, the green emission displays different PL efficiencies (Table 2): in particular, a-CDs have a markedly decreased PLQY with respect to both n-CDs and b-CDs, possibly related to their poor colloidal stability and to the occurrence of aggregation phenomena already discussed above.

Sample	PLQY %
n-CDs	42±5
b-CDs	35±4
a-CDs	8±1

Table 2: Absolute PLQY measured at λ_{exc} = 485nm for the green band of n-CDs, b-CDs and a-CDs.

Finally, a further experiment was made to investigate for a possible redshift of the CDs emission by prolonging the reaction time. In fact, based on the DFT calculations results, an increase in the PAHs conjugation extent, hypothetically occurring for longer reaction time, is expected to result in a smaller HL gap and thus emissions at lower energy. Moreover, a progressive redshift of CDs emission is also expected on the basis of previous reports for CDs synthesized from hydroxybenzenes [12,13]. The CD synthesis was performed in base catalyzed conditions to promote a faster reaction rate while preserving a high colloidal stability of the CDs. Reaction time was prolonged up to 24h, while periodically monitoring the peak position and the FWHM of the PL green band (Figure 8).

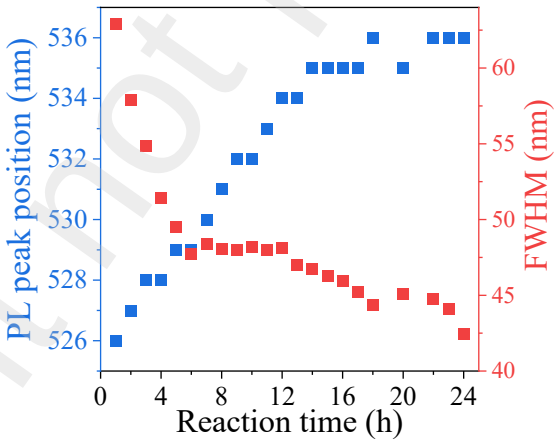

Figure 8: PL peak position (blue dots) and FWHM (red dots) of the b-CDs emission band (λ_{exc} = 485 nm), for reaction times up to 24h.

A small and progressive redshift of only few nm was observed increasing the reaction time up to 14h. Then the spectral position of the peak remained unchanged thereafter, despite the remarkable increase of the polycondensation rate induced by the catalysts. Also, no further decreases in FWHM were observed for prolonged reaction time (>6 h). The absence of redshift of the CDs emission at prolonged reaction times (up to 24 h), might appear in contrast with the seminal works of Yuan et al. [12,13], where an increasingly redshifted emission is obtained by solvothermal route in autoclave by extending the reaction time. This, in turn, suggests that the pressure, the atmosphere composition and in general, the specific experimental conditions of

the synthetic procedure contribute to determine the final optical properties of CDs. On the other hand, at increasing reaction time, when a large number of benzenoid rings are expected to be condensed in PAH, DFT simulation forecasts the formation of distorted and non-planar structures. Such structures are characterized by HL transitions at higher energies, due to the interruption of extended conjugation in the molecule, thus explaining the absence of the red-shift emission at increased reaction time.

3.5 CDs photobleaching resistance

In order to evaluate the resistance of the CD emission to photo-induced degradation processes, the nanoparticles in solution were exposed to continuous UV irradiation (further details on the experimental procedure are provided in Sec.2.8). The b-CDs were selected for this experiment, due to the faster reaction rate and higher reaction yield. Upon UV exposure, O_2 molecules dissolved in ethanol are reasonably expected to form reactive oxygen species (ROSs) that can easily induce degradation reactions, in agreement with previous works on photobleaching of CDs and molecular fluorophores in solution [64].

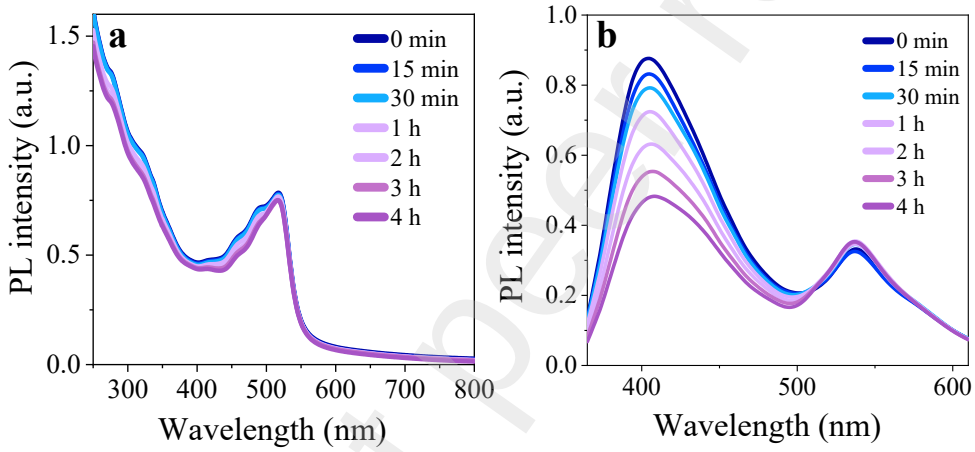

Figure 9: (a) UV-Vis absorption and (b) PL spectra recorded exciting at 350 nm, during the UV-light exposure of b-CDs at progressive irradiation times.

After 4h of UV irradiation, the absorption of b-CDs (Figure 9a) only minimally changed. Instead, the PL bands of b-CDs (Figure 9b) showed a different behavior: at increasing exposure time, the emission intensity of the blue band decreased sensibly, becoming roughly half of its initial value after an irradiation time of 4 h, while the green band remained mainly unaltered.

The results indicate that PAHs in CDs have a high photobleaching resistance. In particular, since both absorption and emission of PAHs exhibit no significant dampening under UV irradiation, we can conclude that PAHs are stable and do not undergo photo-induced degradation during the experiment. On the other hand, for the blue band we observe a strong quenching of the PL emission, without any relevant decrease in its relative absorption (at $\lambda <$ 400 nm). This denotes that UV treatment affects only the sites responsible for radiative recombination, while the absorption states remain almost unaltered. This result is in agreement with the consideration that in CDs emitting from surface states, absorption occurs at the carbogenic core intrinsic states, while radiative recombination arises from discrete states localized at the CD surface [53–55]. In fact, absorption transitions, occurring at the level of the internal core states, are slightly or not at all affected by the UV treatment. Conversely, the CD surface, and hence the sites of the radiative recombination can be more easily involved in photochemical reactions. Then, the ROSs in solution can easily provide degradation of CD

edges or surface chemical groups, resulting in a significative bleaching of their emission [28–30,32].

Following a similar reasoning, if PAHs were located on the CD surface, they also would undergo ROS-induced photobleaching. On the contrary, the preservation of their absorption and green emission, suggests that they are not exposed to ROSs, but rather located in the inner carbonaceous matrix of the CDs, beyond the diffusion length of molecular O_2 or other ROSs [64].

6. Exploiting b-CDs surface charge towards on/off pH sensitive devices

As discussed in the previous sections, the synthesized n-CDs and b-CDs display a negative charge, due to– CO^- groups on their surface; conversely, a-CDs only have a very small positive charge which results in poor stability of the colloidal suspensions. Interestingly, high fluorescence efficiency is only measured for the stable and negatively charged CDs, while a-CDs display much lower PLQY (Table 2). Therefore, it is interesting to analyze more in depth how the fluorescence of CDs is affected by the presence of acid and basic compounds in their surrounding environment. In our experiment, b-CD powder (as obtained after synthesis and purification steps) was disperded in ethanol (4×10^{-3} mg/mL) to form a highly stable colloidal dispersion. Then, different amounts of HCl and NaOH (~ 10 – 100 µmol) were added in alternating steps to 1 mL of CDs solution, while monitoring the intensity of the PAHs green band. As show in Figure 10a, the addition of 20 µmol of HCl provided an almost immediate and strong quenching of the CD fluorescence (PL intensity at 535 nm is around 6% of its initial value). Interestingly, the CD emission was almost fully restored by adding an equimolar amount of NaOH. Then, further quenching was once more caused by adding up to 160 µmol of HCl in three successive steps and again the fluorescence was almost recovered by adding the same amount of base (Figure 10b).

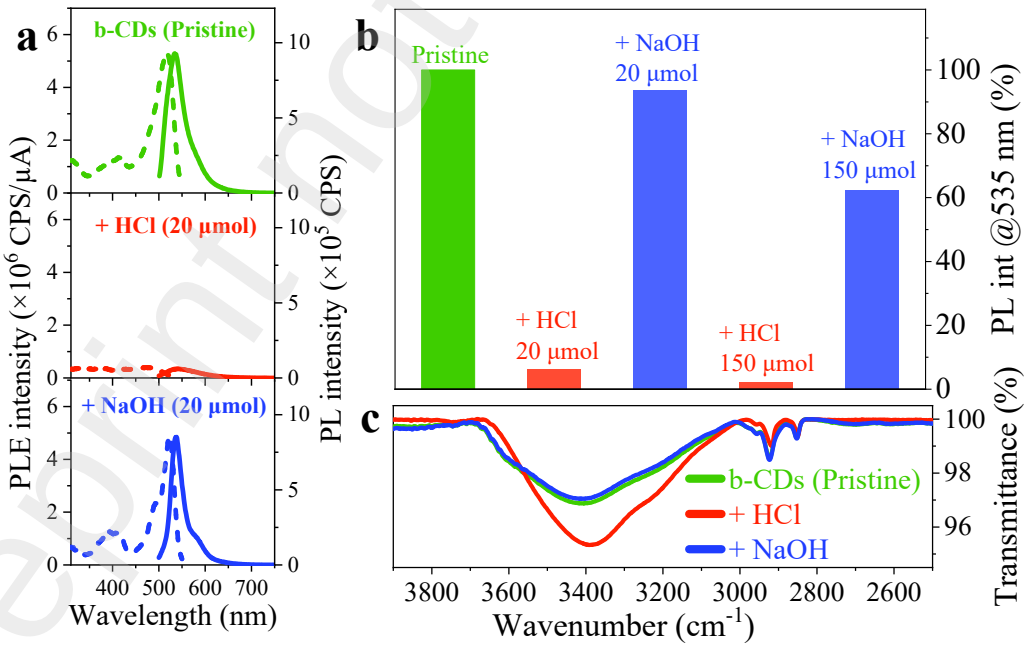

Figure 10: (a) PL excitation (λ_{em} = 585 nm) and emission (λ_{exc} = 485 nm) spectra of b-CDs before and after addition of 20 µmol of HCl and NaOH; (b) PL intensity recorded at 535 nm for pristine b-CDs and after cyclic addition of HCl and NaOH, expressed as percentage of the

initial intensity; (c) O–H stretching band observed in the FT-IR spectra of b-CDs before and after treatment with HCl and NaOH

These results can be explained based on the reversible aggregation of CDs: upon addition of HCl, the surface $–CO^-$ groups of b-CDs get protonated, with the consequent neutralization of their pristine negative surface charge. This can lead to flocculation and formation of weakly emitting aggregates of CDs (as also detected in the absorption spectra recorded during the synthesis of a-CDs, Figure 6b). Indeed, it is well known that CDs suffer from serious self-quenching due to π–π stacking or non-radiative energy transfers in aggregates observed in solution and/or solid state [65]. On the other hand, introducing NaOH restores the electrostatic repulsion among CDs, that are then able to separate and recover their emission properties. The ability of HCl and NaOH to modify the protonation state of the CDs' surface $–CO^-$ groups is further confirmed from the O–H stretching band behavior (Figure 10c). In fact, upon the addition of HCl, b-CDs show a strong –OH band, indicating protonation of the surface $–CO^-$ moieties to C–OH. The next addition of NaOH reversibly restores the intensity of O–H stretching band to that of the pristine b-CDs. These results are also corroborated by the ζ-potential of b-CDs, which shows no change in its average value upon NaOH addition while becoming very close to zero for HCl-added b-CDs (ζ-potential goes from -27.8mV to +0.5 mV).

Finally, it is worth noting that when the process of PL quenching and restoration is cyclically repeated for a certain number of times (Figure 10b), after every restoration with NaOH a low but net loss in emission intensity is observed. This may be ascribed to the fact that, upon addition of NaOH, separation of b-CDs only partially occurs, while some of them remain irreversibly aggregated and hence weakly fluorescent.

The observation of such interesting on/off behavior of the Cs PL, caused by their partly reversible aggregation, paves the way for the use of CDs as sensitive platform for specific acidic/basic compounds, able to selectively quench or restore the CD PL, as well as pH-sensitive smart materials [16,66–71].

4. Conclusions

We synthesized CDs by thermal carbonization of resorcinol in EG in air at atmospheric pressure. During carbon nanoparticle synthesis, fluorescent –OH substituted PAHs are formed from resorcinol polycondensations, and real time spectroscopic monitoring of the reaction, corroborated by a DFT investigation, allowed to analyze their formation and time evolution. In particular, small PAHs arise in the first steps of the reaction, and are further converted into green fluorescent PAHs via addition of aromatic rings. After purification, the synthesized CDs show two emission bands, one in the green (narrow and excitation independent), of PLQY of ~ 40% and ascribed to PAHs and one in the blue (broad and excitation dependent), attributed to CDs' surface state emission.

The resorcinol polycondensations is speeded-up by using NaOH and H_2SO_4 as catalysts. In particular, the acid catalyst yields a very fast carbonization of resorcinol (~ 30 min). However, the a-CDs show poor colloidal stability and low PLQY of green band. Instead, NaOH enables an almost complete resorcinol carbonization within 6 h of reaction, with a large increase of the reaction yield, preserving at the same time the high PLQY of green band and a good colloidal stability.

The resistance to photobleaching has been tested by exposing the b-CDs to prolonged UV irradiation. While surfaces sites, responsible for blue emission, undergo a progressive quenching, the green emission attributed to PAHs was preserved. Such evidence strongly suggests that PAHs are enclosed within the CD carbogenic matrix rather than at their surface edges. Finally, we demonstrate the possibility of cyclically quenching/restoring the green fluorescence by simple addition of a controlled amount of strong acid/base, thus enabling the viable application of the synthesized CDs in sensing technology and smart-materials fabrication.

Funding: This research was funded by the Italian MIUR PRIN 2017 Candl[2] Project Prot. n. 2017W75RAE

Credit author statement

Gianluca Minervini: Conceptualization, Methodology, Investigation, Data Curation, Visualization, Writing – Original Draft **Annamaria Panniello:** Conceptualization, Methodology, Supervision, Writing - Original Draft **Antonino Madonia:** Data Curation, Visualization, Writing – Original Draft **Carlo Maria Carbonaro:** Software, Formal Analysis, Writing – Original Draft **Francesca Mocci:** Software, Formal Analysis, Writing – Original Draft **Teresa Sibillano:** Methodology, Data Curation, Writing – Original Draft **Cinzia Giannini:** Methodology, Data Curation, Writing – Original Draft **Roberto Comparelli:** Resources, Writing – Review & Editing **Chiara Ingrosso:** Resources, Writing – Review & Editing **Nicoletta Depalo:** Resources, Writing – Review & Editing **Elisabetta Fanizza:** Resources, Writing – Review & Editing, **Maria Lucia Curri:** Resources, Writing – Original Draft, **Marinella Striccoli:** Conceptualization, Supervision, Funding Acquisition, Project Administration, Writing – Original Draft

Conflicts of Interest: The authors declare no conflict of interest.

References

[1] K. Hola, Y. Zhang, Y. Wang, E.P. Giannellis, R. Zboril, A.L. Rogach, Carbon dots—Emerging light emitters for bioimaging, cancer therapy and optoelectronics, Nano Today. 9 (2014) 590–603. https://doi.org/10.1016/j.nantod.2014.09.004.

[2] P. Ray, P. Moitra, D. Pan, Emerging theranostic applications of carbon dots and its variants, VIEW. n/a (2021) 20200089. https://doi.org/10.1002/VIW.20200089.

[3] P. Koutsogiannis, E. Thomou, H. Stamatis, D. Gournis, P. Rudolf, Advances in fluorescent carbon dots for biomedical applications, Null. 5 (2020) 1758592. https://doi.org/10.1080/23746149.2020.1758592.

[4] A. Sciortino, A. Cannizzo, F. Messina, Carbon Nanodots: A Review—From the Current Understanding of the Fundamental Photophysics to the Full Control of the Optical Response, C. 4 (2018) 67. https://doi.org/10.3390/c4040067.

[5] Z. Li, L. Wang, Y. Li, Y. Feng, W. Feng, Frontiers in carbon dots: design, properties and applications, Materials Chemistry Frontiers. 3 (2019) 2571–2601. https://doi.org/10.1039/C9QM00415G.

[6] T.H. Kim, W. Wang, Q. Li, Advancement in materials for energy-saving lighting devices, Front. Chem. Sci. Eng. 6 (2012) 13–26. https://doi.org/10.1007/s11705-011-1168-y.

[7] T. Yuan, T. Meng, P. He, Y. Shi, Y. Li, X. Li, L. Fan, S. Yang, Carbon quantum dots: an emerging material for optoelectronic applications, J. Mater. Chem. C. 7 (2019) 6820–6835. https://doi.org/10.1039/C9TC01730E.

[8] M.O. Caglayan, F. Mindivan, S. Şahin, Sensor and Bioimaging Studies Based on Carbon Quantum Dots: The Green Chemistry Approach, Null. (2020) 1–34. https://doi.org/10.1080/10408347.2020.1828029.
[9] N. Gao, L. Huang, T. Li, J. Song, H. Hu, Y. Liu, S. Ramakrishna, Application of carbon dots in dye-sensitized solar cells: A review, Journal of Applied Polymer Science. 137 (2020). https://doi.org/10.1002/app.48443.
[10] S. Iravani, R.S. Varma, Green synthesis, biomedical and biotechnological applications of carbon and graphene quantum dots. A review, Environ Chem Lett. 18 (2020) 703–727. https://doi.org/10.1007/s10311-020-00984-0.
[11] A. Sharma, J. Das, Small molecules derived carbon dots: synthesis and applications in sensing, catalysis, imaging, and biomedicine, Journal of Nanobiotechnology. 17 (2019) 92. https://doi.org/10.1186/s12951-019-0525-8.
[12] F. Yuan, T. Yuan, L. Sui, Z. Wang, Z. Xi, Y. Li, X. Li, L. Fan, Z. Tan, A. Chen, M. Jin, S. Yang, Engineering triangular carbon quantum dots with unprecedented narrow bandwidth emission for multicolored LEDs, Nat Commun. 9 (2018) 2249. https://doi.org/10.1038/s41467-018-04635-5.
[13] F. Yuan, P. He, Z. Xi, X. Li, Y. Li, H. Zhong, L. Fan, S. Yang, Highly efficient and stable white LEDs based on pure red narrow bandwidth emission triangular carbon quantum dots for wide-color gamut backlight displays, Nano Res. 12 (2019) 1669–1674. https://doi.org/10.1007/s12274-019-2420-x.
[14] T. Yoshinaga, M. Shinoda, Y. Iso, T. Isobe, A. Ogura, K. Takao, Glycothermally Synthesized Carbon Dots with Narrow-Bandwidth and Color-Tunable Solvatochromic Fluorescence for Wide-Color-Gamut Displays, ACS Omega. 6 (2021) 1741–1750. https://doi.org/10.1021/acsomega.0c05993.
[15] P. Yang, Z. Zhu, X. Li, T. Zhang, W. Zhang, M. Chen, X. Zhou, Facile synthesis of yellow emissive carbon dots with high quantum yield and their application in construction of fluorescence-labeled shape memory nanocomposite, Journal of Alloys and Compounds. 834 (2020) 154399. https://doi.org/10.1016/j.jallcom.2020.154399.
[16] F. Yan, H. Zhang, N. Yu, Z. Sun, L. Chen, Conjugate area-controlled synthesis of multiple-color carbon dots and application in sensors and optoelectronic devices, Sensors and Actuators B: Chemical. 329 (2021) 129263. https://doi.org/10.1016/j.snb.2020.129263.
[17] M. Moniruzzaman, B. Anantha Lakshmi, S. Kim, J. Kim, Preparation of shape-specific (trilateral and quadrilateral) carbon quantum dots towards multiple color emission, Nanoscale. 12 (2020) 11947–11959. https://doi.org/10.1039/D0NR02225J.
[18] P.D. Khavlyuk, E.A. Stepanidenko, D.P. Bondarenko, D.V. Danilov, A.V. Koroleva, A.V. Baranov, V.G. Maslov, P. Kasak, A.V. Fedorov, E.V. Ushakova, A.L. Rogach, The influence of thermal treatment conditions (solvothermal *versus* microwave) and solvent polarity on the morphology and emission of phloroglucinol-based nitrogen-doped carbon dots, Nanoscale. 13 (2021) 3070–3078. https://doi.org/10.1039/D0NR07852B.
[19] M. Sun, C. Liang, Z. Tian, E.V. Ushakova, D. Li, G. Xing, S. Qu, A.L. Rogach, Realization of the Photostable Intrinsic Core Emission from Carbon Dots through Surface Deoxidation by Ultraviolet Irradiation, J. Phys. Chem. Lett. 10 (2019) 3094–3100. https://doi.org/10.1021/acs.jpclett.9b00842.
[20] J. Wang, C. Cheng, Y. Huang, B. Zheng, H. Yuan, L. Bo, M.-W. Zheng, S.-Y. Yang, Y. Guo, D. Xiao, A facile large-scale microwave synthesis of highly fluorescent carbon dots from benzenediol isomers, J. Mater. Chem. C. 2 (2014) 5028–5035. https://doi.org/10.1039/C3TC32131B.

[21] Y. Lu, J. Wang, H. Yuan, D. Xiao, Separation of carbon quantum dots on a C18 column by binary gradient elution via HPLC, Anal. Methods. 6 (2014) 8124–8128. https://doi.org/10.1039/C4AY01052C.
[22] S. Ghosh, H. Ali, N.R. Jana, Water Dispersible Red Fluorescent Carbon Nanoparticle via Carbonization of Resorcinol, (n.d.) 12.
[23] Y.M. Harshe, G. Storti, M. Morbidelli, S. Gelosa, D. Moscatelli, Modeling Polycondensation of Lactic Acid, Macromol. Symp. 259 (2007) 116–123. https://doi.org/10.1002/masy.200751314.
[24] P.W. Atkins, J. De Paula, Elements of physical chemistry, 5th ed, Oxford University Press, Oxford ; New York, 2009.
[25] G. Minervini, A. Panniello, E. Fanizza, A. Agostiano, M.L. Curri, M. Striccoli, Oil-Dispersible Green-Emitting Carbon Dots: New Insights on a Facile and Efficient Synthesis, Materials. 13 (2020) 3716. https://doi.org/10.3390/ma13173716.
[26] H. Dressler, The Properties and Chemistry of Resorcinol, in: Resorcinol, Springer US, Boston, MA, 1994: pp. 5–25. https://doi.org/10.1007/978-1-4899-0999-2_2.
[27] T. Li, M. Cao, J. Liang, X. Xie, G. Du, Mechanism of Base-Catalyzed Resorcinol-Formaldehyde and Phenol-Resorcinol-Formaldehyde Condensation Reactions: A Theoretical Study, Polymers. 9 (2017) 426. https://doi.org/10.3390/polym9090426.
[28] N. Javed, D.M. O'Carroll, Carbon Dots and Stability of Their Optical Properties, Part. Part. Syst. Charact. 38 (2021) 2000271. https://doi.org/10.1002/ppsc.202000271.
[29] A.V. Longo, A. Sciortino, M. Cannas, F. Messina, UV photobleaching of carbon nanodots investigated by *in situ* optical methods, Phys. Chem. Chem. Phys. 22 (2020) 13398–13407. https://doi.org/10.1039/D0CP00952K.
[30] W. Wang, B. Wang, H. Embrechts, C. Damm, A. Cadranel, V. Strauss, M. Distaso, V. Hinterberger, D.M. Guldi, W. Peukert, Shedding light on the effective fluorophore structure of high fluorescence quantum yield carbon nanodots, RSC Adv. 7 (2017) 24771–24780. https://doi.org/10.1039/C7RA04421F.
[31] R. de Boëver, A. Langlois, X. Li, J.P. Claverie, Graphitic Dots Combining Photophysical Characteristics of Organic Molecular Fluorophores and Inorganic Quantum Dots, JACS Au. 1 (2021) 843–851. https://doi.org/10.1021/jacsau.1c00055.
[32] W. Wang, C. Damm, J. Walter, T.J. Nacken, W. Peukert, Photobleaching and stabilization of carbon nanodots produced by solvothermal synthesis, Phys. Chem. Chem. Phys. 18 (2016) 466–475. https://doi.org/10.1039/C5CP04942C.
[33] M.J. Frisch, G.W. Trucks, H.B. Schlegel, G.E. Scuseria, M.A. Robb, J.R. Cheeseman, G. Scalmani, V. Barone, G.A. Petersson, H. Nakatsuji, X. Li, M. Caricato, A.V. Marenich, J. Bloino, B.G. Janesko, R. Gomperts, B. Mennucci, H.P. Hratchian, J.V. Ortiz, A.F. Izmaylov, J.L. Sonnenberg, Williams, F. Ding, F. Lipparini, F. Egidi, J. Goings, B. Peng, A. Petrone, T. Henderson, D. Ranasinghe, V.G. Zakrzewski, J. Gao, N. Rega, G. Zheng, W. Liang, M. Hada, M. Ehara, K. Toyota, R. Fukuda, J. Hasegawa, M. Ishida, T. Nakajima, Y. Honda, O. Kitao, H. Nakai, T. Vreven, K. Throssell, J.A. Montgomery Jr., J.E. Peralta, F. Ogliaro, M.J. Bearpark, J.J. Heyd, E.N. Brothers, K.N. Kudin, V.N. Staroverov, T.A. Keith, R. Kobayashi, J. Normand, K. Raghavachari, A.P. Rendell, J.C. Burant, S.S. Iyengar, J. Tomasi, M. Cossi, J.M. Millam, M. Klene, C. Adamo, R. Cammi, J.W. Ochterski, R.L. Martin, K. Morokuma, O. Farkas, J.B. Foresman, D.J. Fox, Gaussian 16 Rev. C.01, Wallingford, CT, 2016.
[34] A.D. Becke, Density-functional thermochemistry. III. The role of exact exchange, J. Chem. Phys. 98 (1993) 5648–5652. https://doi.org/10.1063/1.464913.
[35] J. Tirado-Rives, W.L. Jorgensen, Performance of B3LYP Density Functional Methods for a Large Set of Organic Molecules, J. Chem. Theory Comput. 4 (2008) 297–306. https://doi.org/10.1021/ct700248k.

[36] A. Cappai, C. Melis, L. Stagi, P.C. Ricci, F. Mocci, C.M. Carbonaro, Insight into the Molecular Model in Carbon Dots through Experimental and Theoretical Analysis of Citrazinic Acid in Aqueous Solution, J. Phys. Chem. C. 125 (2021) 4836–4845. https://doi.org/10.1021/acs.jpcc.0c10916.
[37] E. Cancès, B. Mennucci, J. Tomasi, A new integral equation formalism for the polarizable continuum model: Theoretical background and applications to isotropic and anisotropic dielectrics, J. Chem. Phys. 107 (1997) 3032–3041. https://doi.org/10.1063/1.474659.
[38] C. Olla, S. Porcu, F. Secci, P.C. Ricci, C.M. Carbonaro, Towards N–N-Doped Carbon Dots: A Combined Computational and Experimental Investigation, Materials. 15 (2022) 1468. https://doi.org/10.3390/ma15041468.
[39] M. Fu, F. Ehrat, Y. Wang, K.Z. Milowska, C. Reckmeier, A.L. Rogach, J.K. Stolarczyk, A.S. Urban, J. Feldmann, Carbon Dots: A Unique Fluorescent Cocktail of Polycyclic Aromatic Hydrocarbons, Nano Lett. 15 (2015) 6030–6035. https://doi.org/10.1021/acs.nanolett.5b02215.
[40] B. Shi, D. Nachtigallová, A.J.A. Aquino, F.B.C. Machado, H. Lischka, Emission Energies and Stokes Shifts for Single Polycyclic Aromatic Hydrocarbon Sheets in Comparison to the Effect of Excimer Formation, J. Phys. Chem. Lett. 10 (2019) 5592–5597. https://doi.org/10.1021/acs.jpclett.9b02214.
[41] M.A. Sk, A. Ananthanarayanan, L. Huang, K.H. Lim, P. Chen, Revealing the tunable photoluminescence properties of graphene quantum dots, J. Mater. Chem. C. 2 (2014) 6954–6960. https://doi.org/10.1039/C4TC01191K.
[42] J. Prakash, A.K. Mishra, Simultaneous Quantification of Multiple Polycyclic Aromatic Hydrocarbons in Aqueous Media using Micelle Assisted White Light Excitation Fluorescence, Sci Rep. 10 (2020) 8921. https://doi.org/10.1038/s41598-020-65788-2.
[43] H.V. Hayes, W.B. Wilson, L.C. Sander, S.A. Wise, A.D. Campiglia, Determination of polycyclic aromatic hydrocarbons with molecular mass 302 in standard reference material 1597a by reversed-phase liquid chromatography and stop-flow fluorescence detection, Anal. Methods. 10 (2018) 2668–2675. https://doi.org/10.1039/C8AY00760H.
[44] W. Brown H., T. Poon, Introduction to organic chemistry, 5th ed., Wiley, 2012.
[45] S. Ramírez-Barroso, A. Jacobo-Martín, I. Navarro-Baena, J.J. Hernández, C. Navio, I. Rodríguez, R. Wannemacher, On the nature of solvothermally synthesized carbon nanodots, J. Mater. Chem. C. 9 (2021) 16935–16944. https://doi.org/10.1039/D1TC04255F.
[46] F. Ehrat, S. Bhattacharyya, J. Schneider, A. Löf, R. Wyrwich, A.L. Rogach, J.K. Stolarczyk, A.S. Urban, J. Feldmann, Tracking the Source of Carbon Dot Photoluminescence: Aromatic Domains versus Molecular Fluorophores, Nano Lett. 17 (2017) 7710–7716. https://doi.org/10.1021/acs.nanolett.7b03863.
[47] E.V. Kundelev, N.V. Tepliakov, M.Yu. Leonov, V.G. Maslov, A.V. Baranov, A.V. Fedorov, I.D. Rukhlenko, A.L. Rogach, Toward Bright Red-Emissive Carbon Dots through Controlling Interaction among Surface Emission Centers, J. Phys. Chem. Lett. 11 (2020) 8121–8127. https://doi.org/10.1021/acs.jpclett.0c02373.
[48] H. Li, X. He, Z. Kang, H. Huang, Y. Liu, J. Liu, S. Lian, C.H.A. Tsang, X. Yang, S.-T. Lee, Water-Soluble Fluorescent Carbon Quantum Dots and Photocatalyst Design, Angewandte Chemie International Edition. 49 (2010) 4430–4434. https://doi.org/10.1002/anie.200906154.
[49] A. Altomare, G. Campi, C. Cuocci, L. Eriksson, C. Giacovazzo, A. Moliterni, R. Rizzi, P.-E. Werner, Advances in powder diffraction pattern indexing: N-TREOR09, J Appl Cryst. 42 (2009) 768–775. https://doi.org/10.1107/S0021889809025503.

[50] D.E. Nixon, G.S. Parry, A.R.J.P. Ubbelohde, Order-disorder transformations in graphite nitrates, Proceedings of the Royal Society of London. Series A. Mathematical and Physical Sciences. 291 (1966) 324–339. https://doi.org/10.1098/rspa.1966.0098.
[51] Z. Gan, H. Xu, Y. Hao, Mechanism for excitation-dependent photoluminescence from graphene quantum dots and other graphene oxide derivates: consensus, debates and challenges, Nanoscale. 8 (2016) 7794–7807. https://doi.org/10.1039/C6NR00605A.
[52] N. Dhenadhayalan, K.-C. Lin, R. Suresh, P. Ramamurthy, Unravelling the Multiple Emissive States in Citric-Acid-Derived Carbon Dots, J. Phys. Chem. C. 120 (2016) 1252–1261. https://doi.org/10.1021/acs.jpcc.5b08516.
[53] V. Nguyen, J. Si, L. Yan, X. Hou, Electron–hole recombination dynamics in carbon nanodots, Carbon. 95 (2015) 659–663. https://doi.org/10.1016/j.carbon.2015.08.066.
[54] A. Sciortino, E. Marino, B. van Dam, P. Schall, M. Cannas, F. Messina, Solvatochromism Unravels the Emission Mechanism of Carbon Nanodots, J. Phys. Chem. Lett. 7 (2016) 3419–3423. https://doi.org/10.1021/acs.jpclett.6b01590.
[55] A. Demchenko, Excitons in Carbonic Nanostructures, C. 5 (2019) 71. https://doi.org/10.3390/c5040071.
[56] H.A. Nguyen, I. Srivastava, D. Pan, M. Gruebele, Unraveling the Fluorescence Mechanism of Carbon Dots with *Sub* -Single-Particle Resolution, ACS Nano. 14 (2020) 6127–6137. https://doi.org/10.1021/acsnano.0c01924.
[57] K. Jiang, S. Sun, L. Zhang, Y. Lu, A. Wu, C. Cai, H. Lin, Red, Green, and Blue Luminescence by Carbon Dots: Full-Color Emission Tuning and Multicolor Cellular Imaging, Angewandte Chemie International Edition. 54 (2015) 5360–5363. https://doi.org/10.1002/anie.201501193.
[58] H. Ding, S.-B. Yu, J.-S. Wei, H.-M. Xiong, Full-Color Light-Emitting Carbon Dots with a Surface-State-Controlled Luminescence Mechanism, ACS Nano. 10 (2016) 484–491. https://doi.org/10.1021/acsnano.5b05406.
[59] J.R. Lakowicz, Principles of Fluorescence Spectroscopy, 3rd ed., Springer US, 2006. https://doi.org/10.1007/978-0-387-46312-4.
[60] J.A. Snyder, P. Grüninger, H.F. Bettinger, A.E. Bragg, Excited-State Deactivation Pathways and the Photocyclization of BN-Doped Polyaromatics, J. Phys. Chem. A. 121 (2017) 5136–5146. https://doi.org/10.1021/acs.jpca.7b04878.
[61] J.M. Alvarez-Pez, L. Ballesteros, E. Talavera, J. Yguerabide, Fluorescein Excited-State Proton Exchange Reactions: Nanosecond Emission Kinetics and Correlation with Steady-State Fluorescence Intensity, J. Phys. Chem. A. 105 (2001) 6320–6332. https://doi.org/10.1021/jp010372+.
[62] E. Martin, M. Prostredny, A. Fletcher, Investigating the Role of the Catalyst within Resorcinol–Formaldehyde Gel Synthesis, Gels. 7 (2021) 142. https://doi.org/10.3390/gels7030142.
[63] S. Mulik, C. Sotiriou-Leventis, N. Leventis, Time-Efficient Acid-Catalyzed Synthesis of Resorcinol−Formaldehyde Aerogels, Chem. Mater. 19 (2007) 6138–6144. https://doi.org/10.1021/cm071572m.
[64] A.P. Demchenko, Photobleaching of organic fluorophores: quantitative characterization, mechanisms, protection, Methods Appl. Fluoresc. 8 (2020) 022001. https://doi.org/10.1088/2050-6120/ab7365.
[65] J. Wang, Y. Yang, X. Liu, Solid-state fluorescent carbon dots: quenching resistance strategies, high quantum efficiency control, multicolor tuning, and applications, Materials Advances. 1 (2020) 3122–3142. https://doi.org/10.1039/D0MA00632G.
[66] M. Zheng, Z. Xie, D. Qu, D. Li, P. Du, X. Jing, Z. Sun, On–Off–On Fluorescent Carbon Dot Nanosensor for Recognition of Chromium(VI) and Ascorbic Acid Based on the Inner

Filter Effect, ACS Appl. Mater. Interfaces. 5 (2013) 13242–13247. https://doi.org/10.1021/am4042355.
[67] H. Yang, Y. Liu, Z. Guo, B. Lei, J. Zhuang, X. Zhang, Z. Liu, C. Hu, Hydrophobic carbon dots with blue dispersed emission and red aggregation-induced emission, Nature Communications. 10 (2019) 1–11. https://doi.org/10.1038/s41467-019-09830-6.
[68] C. Wang, K. Jiang, Q. Wu, J. Wu, C. Zhang, Green Synthesis of Red-Emitting Carbon Nanodots as a Novel "Turn-on" Nanothermometer in Living Cells, Chemistry – A European Journal. 22 (2016) 14475–14479. https://doi.org/10.1002/chem.201602795.
[69] P. Singhal, B.G. Vats, S.K. Jha, S. Neogy, Green, Water-Dispersible Photoluminescent On–Off–On Probe for Selective Detection of Fluoride Ions, ACS Appl. Mater. Interfaces. 9 (2017) 20536–20544. https://doi.org/10.1021/acsami.7b03346.
[70] Y.Z. Yang, N. Xiao, S.G. Liu, L. Han, N.B. Li, H.Q. Luo, pH-induced aggregation of hydrophilic carbon dots for fluorescence detection of acidic amino acid and intracellular pH imaging, Materials Science and Engineering: C. 108 (2020) 110401. https://doi.org/10.1016/j.msec.2019.110401.
[71] A.-Q. Xie, J. Guo, L. Zhu, S. Chen, Carbon dots promoted photonic crystal for optical information storage and sensing, Chemical Engineering Journal. 415 (2021) 128950. https://doi.org/10.1016/j.cej.2021.128950.